SCIENTIFIC REPORTS

OPEN

SUBJECT AREAS:
PHOTONIC CRYSTALS
SOLAR CELLS

Received
9 May 2014

Accepted
26 August 2014

Published
23 September 2014

Correspondence and requests for materials should be addressed to K.X. (nwpuxky@163.com) or H.H. (aphhuang@polyu.edu.hk)

* These authors contributed equally to this work.

Aperiodic TiO_2 Nanotube Photonic Crystal: Full-Visible-Spectrum Solar Light Harvesting in Photovoltaic Devices

Min Guo[1]*, Keyu Xie[2]*, Yu Wang[1,3], Limin Zhou[4] & Haitao Huang[1]

[1]Department of Applied Physics and Materials Research Center, The Hong Kong Polytechnic University, Hung Hom, Kowloon, Hong Kong, [2]State Key Laboratory of Solidification Processing and Center for Nano Energy Materials and School of Materials Science and Engineering, Northwestern Polytechnical University, Xi'an 710072, P.R. China, [3]Hong Kong Polytechnic University Shenzhen Research Institute, Shenzhen, China, [4]Department of Mechanical Engineering, The Hong Kong Polytechnic University, Hung Hom, Kowloon, Hong Kong.

Bandgap engineering of a photonic crystal is highly desirable for photon management in photonic sensors and devices. Aperiodic photonic crystals (APCs) can provide unprecedented opportunities for much more versatile photon management, due to increased degrees of freedom in the design and the unique properties brought about by the aperiodic structures as compared to their periodic counterparts. However, many efforts still remain on conceptual approaches, practical achievements in APCs are rarely reported due to the difficulties in fabrication. Here, we report a simple but highly controllable current-pulse anodization process to design and fabricate TiO_2 nanotube APCs. By coupling an APC into the photoanode of a dye-sensitized solar cell, we demonstrate the concept of using APC to achieve nearly full-visible-spectrum light harvesting, as evidenced by both experimental and simulated results. It is anticipated that this work will lead to more fruitful practical applications of APCs in high-efficiency photovoltaics, sensors and optoelectronic devices.

The concept of photon management has emerged as one of the hottest research topics in the effort to enhance light harvesting efficiencies in photovoltaics, sensors and optoelectronic devices[1–4]. Intensive studies have been made in recent years to scrupulously design hierarchically ordered nanoarchitectures[5,6], or to integrate plasmonic and/or photonic structures in such devices for efficient light management, both theoretically and experimentally[7–10]. For example, by collective oscillations of free electrons localized at surfaces of metallic nanostructures, plasmonics has been used to enhance light harvesting in various types of solar cells, such as silicon solar cells[11], CdTe solar cells[12], organic solar cells[13], and dye-sensitized solar cells (DSSCs)[14]. As a promising alternative, photonic crystals (PCs) with periodic dielectric nanostructures, which are able to trap and slow photons in the light absorbing layer, have also been successfully integrated in solar cells to improve the light harvesting efficiency[15–20]. Various approaches, such as, nanopatterning[21], template-assisted[22] and layer-by-layer assembly techniques[23], are often used to design and fabricate PCs with various spatial nanostructures. A novel TiO_2 nanotube PC (NTPC) with freely tunable bandgap was recently fabricated by a current-pulse anodization method[24–26]. The NTPC made by this technique shows the great potential to be applied to DSSCs for significantly enhanced light harvesting by proper selection of the bandgap[24,25].

However, PC with a periodic structure shows a strong reflection of light only in a relatively narrow range. To maximize the light harvesting, a strong light reflection over a broader range is preferred. From the structural point of view, this requires a spatial variation of the periodicity where the PC can be called aperiodic PC (APC)[27]. Study on APCs with aperiodic sequences, such as, Fibonacci, Cantor, Thue-Morse, and Rudin-Sphapiro, were originally driven by mathematical motivations and previous work was mainly theoretical[28]. Experimentally, due to the lack of an efficient fabrication technique to deal with the extremely complex spatial structure, the existence of large amount of structural defects makes the APCs difficult to accurately display the desired properties[27,29–31]. Thus, the experimental exploration of APCs for real device applications is rarely reported.

By using a current-pulse anodization process with diminishing time period, we demonstrate the successful fabrication of TiO_2 nanotube APCs (NTAPCs). Compared to the conventional approaches, such as template-assisted and layer-by-layer assembly techniques, this method is simple, highly controllable and economical. As a proof-of-concept, we couple the TiO_2 NTAPC to the photoanode of DSSC and, due to the broadband reflectance in APC with an arithmetic sequence, an increase of 27.01% in photocurrent can be observed. Enhanced light

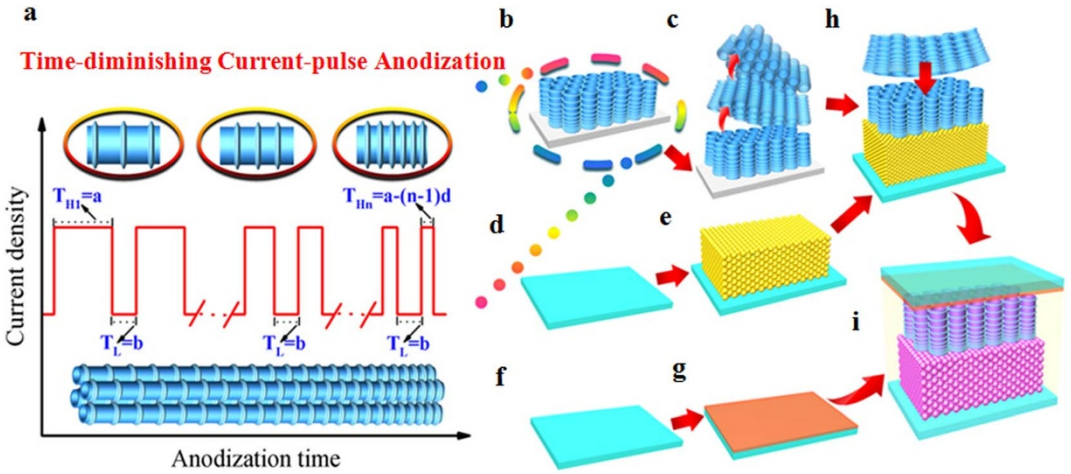

Figure 1 | Schematic illustration of the fabrication of a TiO_2 NTAPC coupled DSSC. (a) The time-diminishing current-pulse anodization process for TiO_2 NTAPC. (b) Formation of TiO_2 NTAPC membrane. (c) Self-detachment of the NTAPC membrane from the Ti substrate by anodization at 70V. (d), (e) Doctor-blade coating of TiO_2 nanoparticle paste on FTO. (f), (g) The conventional preparation process of Pt-coated FTO by thermal decomposition. (h) Attachment of the TiO_2 NTAPC membrane onto the TiO_2 nanoparticle paste by calcination at 450°C. (i) Final assembly of the TiO_2 NTAPC coupled DSSC.

harvesting in nearly full-visible-spectrum from purple to red is verified by numerical simulations and systematic experimental studies. It is believed that our work on TiO_2 NTAPC with broadband reflectance will open a door for more fabrication methods of APCs to appear, and eventually bring about more practical applications of APCs in a variety of photonic devices.

Results and discussion

The TiO_2 NTAPC coupled photoanode, consisting of a membrane of TiO_2 NTAPC and a layer of TiO_2 nanoparticle (NP), was assembled into a cell following the process described in Figure 1. First, the TiO_2 NTAPC with a gradually decreasing lattice constant (in an arithmetic sequence) was obtained by time-diminishing current-pulse anodization (Figure 1a, b). Then, a self-detaching anodization (Figure 1c) was applied to form a free-standing TiO_2 NTAPC membrane with high quality optical properties. Next, the detached TiO_2 NTAPC membrane was transferred and attached onto a transparent FTO substrate (Figure 1h) coated with a thick (~8 μm) absorbing layer of TiO_2 NPs via a doctor-blade method (Figure 1d, e). Finally, the photoanode was annealed and assembled with a thermal adhesive film and Pt-coated counter electrode (Figure 1f, g) to form a sandwich type cell (Figure 1i).

The most challenging part of the work is to accurately control the lattice constant of the TiO_2 NTAPC in order to achieve the desired features. This can be achieved by controlling the time duration of anodization current pulse, since the lattice constant of the TiO_2 PC layer is in a linear relationship with the time duration of a high-current (HC) pulse[24,25]. In this work, the TiO_2 NTAPC with a gradually decreasing lattice constant (in arithmetic sequence) was fabricated by a time-diminishing current-pulse anodization method, where the time duration of the HC pulse was decreased gradually following an arithmetic sequence (Figure 1a and Supporting Information Figure S1). The lattice constant of the TiO_2 NTAPC membrane decreased almost linearly from ~230 nm on the top to ~180 nm in the middle and ~110 nm on the bottom, respectively (Figure 2).

The working principle of the TiO_2 NTAPC coupled photoanode to achieve the full visible spectrum solar light harvesting is schematically illustrated in Figure 3a. When the photoanode was illuminated from the front side, the non-absorbed incident light within the visible range would be reflected back to the TiO_2 NP absorbing layer by the TiO_2 NTAPC layer and hence enhanced photon harvesting can be anticipated.

The experimental and simulated reflectance spectra of the TiO_2 NTAPC/NP photoanode in air and ethanol are shown in Figure 3c. Compared to the reflection spectra of a photoanode coupled with a PC (TiO_2 NTPC/NP, Supporting Information Figure S2), which shows a narrow reflection peak at about 450 and 510 nm in air and ethanol, respectively, the reflection spectra of TiO_2 NTAPC/NP photoanode show a broader peak from 400 to 650 nm in air and from 400 to 750 nm in ethanol. The experimental results agree quite well with the simulated reflectance spectra of the TiO_2 NTAPC/NP photoanode in terms of the peak position. The origin of the reflectance peak broadening in NTAPC can be easily understood by viewing the APC as a stack of PC layers with different lattice parameters. Each PC layer reflects light with a peak at its Bragg position. The reflectance peak shifts continuously as the lattice parameter gradually changes in an arithmetic sequence. The reflectance peaks from different layers superimpose to form broader peaks with increased peak maximum, until it reaches 100%. In the present study, the thickness of the ith ($i = 1, 2, \ldots, 32$) unit cell in the NTAPC layer, which contains a protruded ring, and a normal tube with certain length, can be expressed as $b_i = b_1 + (i-1)d$, where d is the common difference (3.6 nm in this study) of the arithmetic sequence, and b_1 is the initial term, the thickness of the first unit cell. Figure 3b shows the simulated reflection peaks from two 8-unit-cell NTAPC slabs, one with $b_1 = 165.2$ nm and the other 194 nm. When they superimpose, (i.e., forming a 16-unit-cell slab) the reflection peak is greatly broadened to 475–655 nm, covering the two stop bands of each individual 8-unit-cell slab (i.e., 470–595 nm and 540–670 nm, respectively). At the same time, the reflection peak also increases in intensity and becomes flattened when the intensity reaches 100% in the range of 535–610 nm. When two 16-unit-cell slabs are further stacked to form a 32-unit-cell NTAPC slab, the desired strong reflection with a value of almost 100% can be obtained in a range of 400 to 600 nm.

To have a thorough understanding of the effect of TiO_2 NTAPC on the light harvesting of a DSSC, the spatial distribution of the amplitude of the electric field at four different wavelengths, namely, 405, 515, 674 and 783 nm, are plotted in Figure 3d. It can be seen that, at a wavelength of 405 nm, the TiO_2 NTAPC acts as a Bragg mirror to reflect photons back to the TiO_2 NP absorbing layer. The reflection mainly takes place at the interface between the TiO_2 NTAPC and TiO_2 NP layers and it causes strong photon resonance modes in the TiO_2 NP layer. As the wavelength is increased from 515

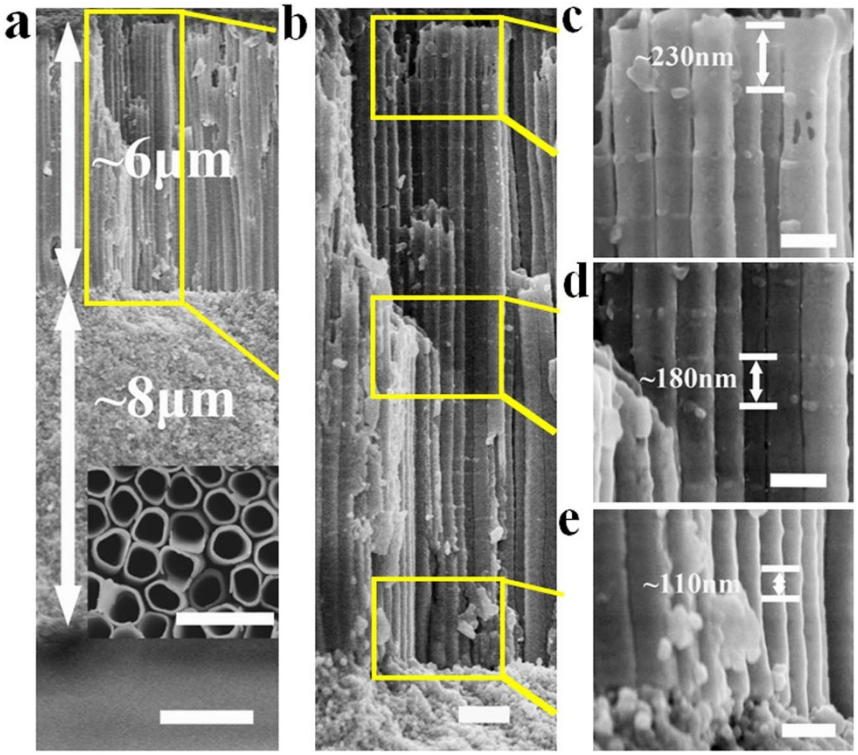

Figure 2 | The morphology and structure of the TiO_2 NTAPC/NP photoanode. (a) FESEM image showing the cross-section of a photoanode (the TiO_2 NTAPC with 35 periods and the TiO_2 NP are ~6 and 8 μm in thickness, respectively). Inset: top-view of the TiO_2 NTAPC. (b) Magnified view of the TiO_2 NTAPC. (c), (d), (e) Magnified views of the TiO_2 NTAPC shown in (b) (top, middle and bottom parts, respectively). The scale bar measures 2 μm for (a), 500 nm for inset of (a), 500 nm for (b), 200 nm for (c), (d) and (e).

to 674 nm and finally to 783 nm, the reflection interface gradually shifts towards the longer lattice constant side (i.e., the left side of Figure 3d), which corresponds to Bragg reflection at longer wavelength (as shown in Figure 3b). As compared to the electric field distribution in a photoanode coupled with TiO_2 NTPC (with a fixed lattice constant of 150 nm, Supporting Information Figure S3), the stronger electric field observed in the NTAPC layer indicates that the NTAPC also contributes to the light harvesting. The contribution from NTAPC is more significant at longer wavelength. As the wavelength increases, the electric field penetrates more deeply into the NTAPC layer (Figure 3d). This also manifests the importance of choosing TiO_2 as the material for NTAPC.

The photocurrent vs. voltage curves of the NTAPC coupled cell were compared with two reference cells integrated with smooth TiO_2 NTs and TiO_2 150NTPC (NTPC with fixed lattice constant of 150 nm), respectively (Figure 4a). The 150NTPC was chosen as a reference since its reflectance maximum best matches the absorption maximum of N719 dye. The photoanodes of all the cells have the same total thickness of ~14 μm (Supporting Information Figure S4). An 8-μm-thick absorbing layer is chosen for a higher power conversion efficiency as compared to a thinner absorbing layer (Supporting Information Figure S5). The corresponding photovoltaic parameters, extracted from *I–V* curves shown in Figure 4a, are summarized in Table 1. The three different cells show similar fill factor (*FF*) and open circuit voltage (V_{oc}). However, large and substantial variations of the short-circuit current density (J_{sc}) can be observed in different cells.

The J_{sc} of the reference cell with TiO_2 NT/NP photoanode reaches 14.07 $mA \cdot cm^{-2}$. By coupling the photoanode with 150NTPC, an increase of 16.56% in J_{sc} can be obtained. By coupling the photoanode with an NTAPC layer (instead of the 150NTPC), a greater increase in J_{sc} (27.01%) is achieved. The power conversion efficiency (η) of the NTAPC coupled cell has reached 7.87%, which is one of the highest values reported for all sorts of PC-coupled DSSCs to date (Supporting Information Table S1).

Light harvesting enhancement in the whole visible range in the cell coupled with NTAPC can be clearly seen from the incident photon-to-electron conversion efficiency (IPCE) measurement (Figure 4b). IPCE of a DSSC can be expressed as a product of the light harvesting efficiency (η_{LH}), the electron injection efficiency (η_{INJ}), and the electron collection efficiency (η_{COL}), i.e., $\eta_{IPCE}(\lambda) = \eta_{LH}(\lambda) \times \eta_{INJ}(\lambda) \times \eta_{COL}(\lambda)$, all of which are wavelength dependent[32]. Among them, η_{LH} is determined by the amount of dye loading, the photon management ability of the photoanode, and other factors; η_{INJ} is largely determined by the competition between charge recombination and charge collection; η_{COL} mainly depends on the interface situation of absorbed dye on the photoanode material[33]. The electron lifetimes (τ_r, obtained from the electrochemical impedance spectroscopy, Supporting Information Figure S6) of the three different types of photoanodes are quite similar as shown in Table 1, showing similar dynamics. The electron collection efficiencies of different cells tested in the present work can also be assumed to be the same, due to the same dye and the same materials used in different types of DSSCs. Hence, in the present study, the improved IPCE in NTAPC coupled cell is mainly due to the enhanced light harvesting efficiency, i.e., the enhanced absorptance, leading to increased J_{sc}. Indeed, the introduction of TiO_2 150NTPC only result in the increase of IPCE over a relatively narrow wavelength range, because of the narrow bandwidth of TiO_2 150NTPC. While for the cell equipped with the TiO_2 NTAPC photoanode, the IPCE value is significantly greater than those cells coupled with smooth TiO_2 NT or TiO_2 150NTPC over almost the whole visible spectrum. The enhancement of IPCE over such a broad wavelength range in NTAPC coupled cell clearly demonstrates the important role played APC to achieve full-visible-spectrum solar light harvesting.

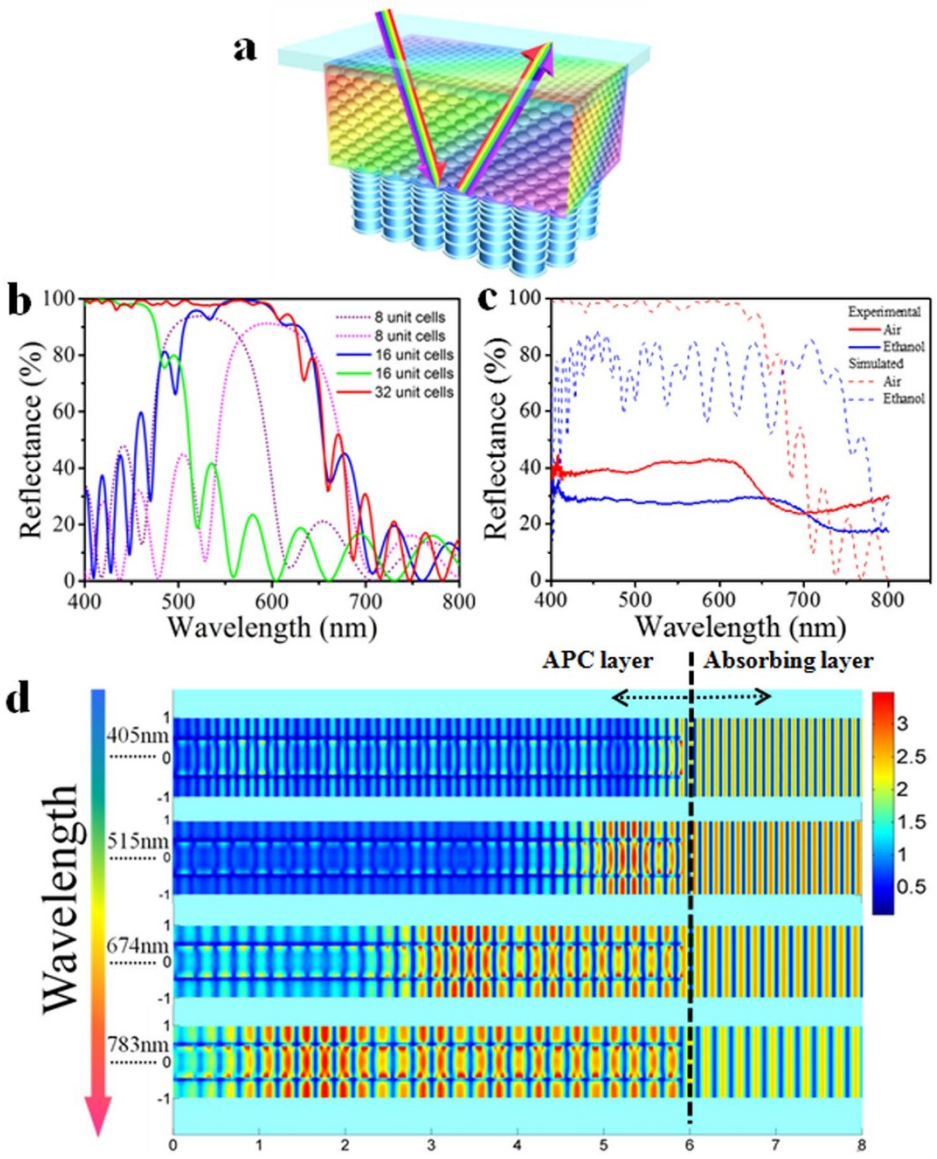

Figure 3 | Experimental and simulated optical properties of TiO_2 NTAPC coupled photoanode. (a) Light trapping in the NTAPC coupled photoanode. (b) Simulated reflectance spectra of NTAPC with different number of unit cells showing the spectrum broadening effect. The reflectance spectra of two 8-unit-cell NTAPC slabs with b_1 = 165.2 and 194 nm are shown as dotted lines in purple and pink, respectively. The green and blue solid lines are the reflectance from two 16-unit-cell NTAPC slabs with b_1 = 107.6 and 165.2 nm, respectively. The red solid line is the reflectance curve from a 32-unit-cell NTAPC slab with b_1 = 107.6 nm. (c) Experimental and simulated reflectance spectra (under near normal incidence) of the TiO_2 NTAPC coupled photoanode in air and ethanol, respectively. The background reflectance from the FTO coated glass substrate covered with TiO_2 NPs was subtracted. (d) Distribution of the amplitude of the electric field in different parts of the photoanode.

Numerical simulations (Figure 4c) of the absorptance of the DSSCs show that the cell coupled with 150NTPC has an enhanced absorption mainly around the Bragg position (~510 nm) of 150NTPC immersed in electrolyte. An appreciable increase in simulated absorptance in almost the whole visible range can be found in cells coupled with NTAPC. These results are in accordance with the measured IPCE. In addition, the percentage enhancement in J_{sc} based on theoretical simulation ($S\Delta J_{sc}/J_{sc}$) also agrees well with the one obtained from experiments ($E\Delta J_{sc}/J_{sc}$). The $S\Delta J_{sc}/J_{sc}$ of TiO_2 NTAPC/NP and TiO_2 150NTPC/NP is 23.04 and 11.08%, respectively, while the $E\Delta J_{sc}/J_{sc}$ of TiO_2 NTAPC/NP and TiO_2 150NTPC/NP is 27.01 and 16.56%, respectively. The slight difference between the experimental and simulated results can be ascribed to the difference in the amount of dye loading in different photoanodes (Table 1). Due to the protruding rings around the smooth nanotubes, the NTPC/NP and NTAPC/NP photoanodes normally have slightly larger surface area than the NT/NP photoanode, and hence higher amounts of dye loading. Thus, it can be concluded that the enhanced J_{sc} is mainly attributed to the full-visible-spectrum solar harvesting achieved by TiO_2 NTAPC.

In conclusion, we have developed a novel versatile technology, enabling precise fabrication and tailoring of the complex spatial structure of TiO_2 NTAPC with wide and tunable reflection spectrum to achieve high-efficiency photon management. The impact of this work will go far beyond just a proof-of-concept of nearly full-visible-spectrum solar light harvesting by integrating TiO_2 NTAPC into DSSCs to reach 27.0% increase in J_{sc} and an efficiency of 7.87%. Our strategy allows multi-degree of freedoms in the design of nanostructures for the exploration of a plethora of fascinating properties of APC for practical applications in photonics.

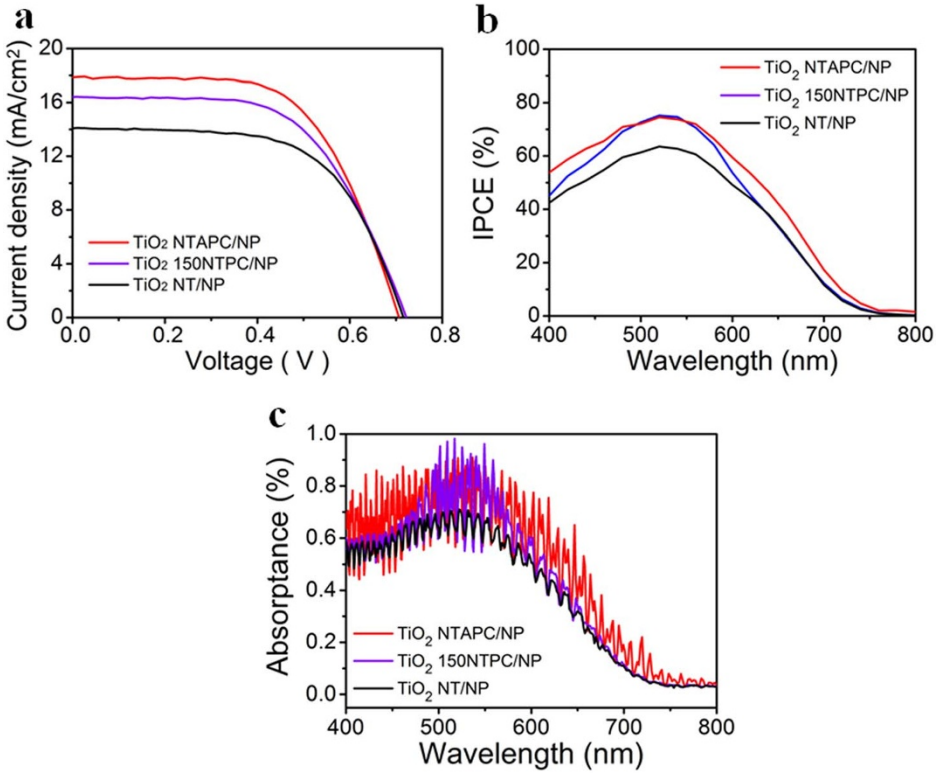

Figure 4 | Photovoltaic performance of TiO_2 NTAPC-coupled DSSC. (a) Photocurrent-voltage curves of three representative cells: TiO_2 NTAPC/NP, TiO_2 150NTPC/NP, and TiO_2 NT/NP. The TiO_2 NP layer has a thickness of 8 μm. The TiO_2 NTAPC, TiO_2 150NTPC and TiO_2 NT layers have the same thickness of 6 μm, (b), (c) Experimental IPCE and numerical simulated absorptance, respectively, of the three representative DSSCs.

Methods

Materials and Reagents. All materials and reagents were used as received without further purification or treatment. Titanium foils (99.7%) were purchased from Strem Chemical (USA). Ethylene glycol (EG, 99.5%), ammonium fluoride (96%), acetone, and ethanol were obtained from International Laboratory (USA). D.I. water (18.2 MΩ·cm) was produced by Direct-Q 3 Water Purification Systems (Millipore). The FTO glass (Nippon Sheet Glass), Pt-coated FTO glass, thermal adhesive film (25 μm thick, Surlyn-1702), N719 dye (Solaronix) and the electrolyte (DMPD: 1.0 M, LiI: 0.1 M, 4-TBP: 0.5 M, I_2: 0.12 M, 3-methoxy propionitrile) were purchased from Wuhan Geao Instruments Science and Technology Co. Ltd (China). The TiO_2 NP paste (20 nm, 18NR-T) was purchased from Dyesol (Australia).

Fabrication of TiO_2 NTAPC. The TiO_2 NTAPC was fabricated by time-diminishing current-pulse anodization. Briefly, the titanium foils were pre-treated by anodization at 70 V for 10 min, using an electrolyte consisting of 0.5 wt% ammonium fluoride in an aqueous EG solution (3 vol% D.I. water in EG) in a two-electrode electrochemical cell. Then the flat Ti surface was subject to a subsequent ultrasonic treatment in D.I. water for 5–10 min. Current pulse anodization with alternating high current (HC) and low current (LC) pulses was then adopted to fabricate the TiO_2 NTAPC. The current density of the HC pulse was so determined to achieve an anodization voltage of around 70 V. The time duration for LC pulse was fixed at 90 s, while that for the HC pulse started from 40 s, and then decreased in an arithmetic sequence to 16 s after 35 cycles. For all the samples, the thickness of TiO_2 NTAPC membrane was fixed to ~6 μm.

Fabrication of the Photoanodes and DSSCs. To construct the proposed photoanode (TiO_2 NTAPC/NP), the as-grown TiO_2 NTAPC membrane was firstly heat treated at 270 °C for 1 h. Then it was detached with a subsequent anodization at a bias voltage of 60 V for 2 h in the same electrolyte as reported in our previous work[24,25]. After being washed with ethanol, the TiO_2 NTAPC membrane was detached from the titanium substrate, and then adhered to the FTO substrate with TiO_2 NP paste via a doctor-blade method. The adhered samples were then annealed at 450 °C for 3 h under heating and cooling rates of 1 °C min^{-1}. The photoanodes were then soaked in a dye-containing solvent (0.3×10^{-3} M N719 in ethanol) at 60 °C for 24 h, followed by rinsing in pure ethanol for 1 min to remove non-chemisorbed dye. Subsequently, the dye-sensitized TiO_2 electrode and Pt-counter electrode were assembled into a sandwich type cell and sealed with a thermal adhesive film. The electrolyte was infiltrated into the cells by placing the electrolyte droplet in the cavity of the active area of the device before it was sealed with UV epoxy. In this study, TiO_2 NT/NP and TiO_2 150NTPC/NP reference photoanodes were also made, with the thickness of TiO_2 NT and 150NTPC layers the same as that of the TiO_2 NTAPC layer. For each type of cells, more than 5 samples were made and characterized.

Characterization of the Photoanodes and DSSCs. Reflectance spectra were acquired using a typical microreflectivity/microtransmission system (Ocean Optics(R) USB2000+ fiber spectrometer) over a sample area of roughly 5×5 μm² with a magnification of 100×. A spectral range of 400–800 nm was explored using a tungsten-halogen lamp. A field emission scanning electron microscope (FESEM, JEOL JSM-6335F) was used to study the microstructure. I–V characteristics were measured using a Keithley 2420 source meter. For white-light efficiency measurements (at 100 mW·cm^{-2}), a Newport 91160 solar-light simulator with an AM 1.5 filter was used. All the measurements were performed in air over an active area of 0.16 cm^2. For IPCE measurement, the light source was from a Newport 66902 solar simulator. The wavelength of light was tuned with a Newport 74125 monochromator. The photocurrent was measured with a Newport 2931-C power meter. The light intensity was measured with a Newport 2931-C power meter equipped with a 71675_71580 detector probe. The electrochemical impedance spectroscopy (EIS) data were collected at the open circuit voltage with an AC perturbation signal of an amplitude of 10 mV and a frequency within 0.05 to 10^5 Hz. Dye amounts were determined by desorption the photoanodes in 0.1 M NaOH

Table 1 | Characteristic photovoltaic parameters of the samples. $E\Delta J_{sc}/J_{sc}$ and $S\Delta J_{sc}/J_{sc}$ are the percentage enhancement in J_{sc} based on experimental and theoretical simulation results (TiO_2 NT/NP as the reference), respectively

Photoanode	V_{oc} (V)	J_{sc} (mA·cm^{-2})	*FF*	η (%)	$E\Delta J_{sc}/J_{sc}$ (%)	$S\Delta J_{sc}/J_{sc}$ (%)	Dye loading (nmol·cm^{-2})	τ_r (ms)
TiO_2 NT/NP	0.71	14.07	0.62	6.19	-	-	136	9.0
TiO_2 150NTPC/NP	0.72	16.40	0.61	7.20	16.56	11.08	147	9.7
TiO_2 NTAPC/NP	0.71	17.87	0.62	7.87	27.01	23.04	148	9.5

aqueous solution and measuring the absorbance by a UV-Vis spectrophotometer (Model UV-2550, Shimadzu, Japan).

Simulation and Theoretical Calculation. The numerical calculation of both reflection and absorption spectra were performed with finite-element full wave simulation method. Similar to the experiments, in our models, the incoming light first incident normally on a conductive transparent substrate (refractive index $n_1 = 1.45$), on which an 8 μm thick TiO_2 NP layer with 50% porosity has been deposited. The effective refractive index of this layer, assuming that the electrolyte (with $n = 1.403$, similar to that of 3-methoxy propionitrile electrolyte) fills all the pores, is $n_3 = 2.03$. The light then reaches the TiO_2 150NTPC or TiO_2 NTAPC layer (~6 μm in thickness), modelled as TiO_2 NTs arranged in a hexagonal lattice with the geometric features similar to the experimental samples, i.e., the outer diameter and the wall thickness being 110 and 10 nm, respectively, with the axial direction of NTs perpendicular to the conducting substrate. In addition, periodic boundary conditions were adopted in our simulation to allow the simulation of the nanotube array. All the layers of the photoanode, including NP, NT, PC, and APC layers of TiO_2, were sensitized by ruthenium dye N719, and the absorption coefficient of the ruthenium dye, which is represented by the frequency-dependent imaginary part of the complex refractive index, is obtained by fitting photocurrent and absorptance spectra of similar TiO_2 NP layer and device. Finally, the electrolyte was considered as the last media in our model. The refractive indices of different layers were calculated by the effective medium theory, using $n_{TiO2} = 2.51$. More details about the simulation and theoretical calculation can be found in the Supporting Information.

1. Polman, A. & Atwater, H. A. Photonic design principles for ultrahigh-efficiency photovoltaics. *Nat. Mater.* **11**, 174–177 (2012).
2. Kim, J. B. *et al.* Wrinkles and deep folds as photonic structures in photovoltaics. *Nat. Photon.* **6**, 327–332 (2012).
3. Stanley, R. Plasmonics in the mid-infrared. *Nat. Photon.* **6**, 409–411 (2012).
4. Nelson, E. C. *et al.* Epitaxial growth of three-dimensionally architectured optoelectronic devices. *Nat. Mater.* **10**, 676–681 (2011).
5. Wu, W. Q. *et al.* Maximizing omnidirectional light harvesting in metal oxide hyperbranched array architectures. *Nat. Common.* **5**, 3968 (2014).
6. Lei, X. B. *et al.* Ordered crystalline TiO_2 nanotube arrays on transparent FTO glass for efficient dye-sensitized solar cells. *J. Phys. Chem. C.* **114**, 15228–15233 (2010).
7. Leung, S.-F. *et al.* Efficient photon capturing with ordered three-dimensional nanowell arrays. *Nano Lett.* **12**, 3682–3689 (2012).
8. Aubry, A. *et al.* Plasmonic light-harvesting devices over the whole visible spectrum. *Nano Lett.* **10**, 2574–2579 (2010).
9. Chanda, D. *et al.* Coupling of plasmonic and optical cavity modes in quasi-three-dimensional plasmonic crystals. *Nat. Commun.* **2**, 479 (2011).
10. Spinelli, P., Verschuuren, M. A. & Polman, A. Broadband omnidirectional antireflection coating based on subwavelength surface Mie resonators. *Nat. Commun.* **3**, 692 (2012).
11. Pillai, S., Catchpole, K. R., Trupke, T. & Green, M. A. Surface plasmon enhanced silicon solar cells. *J. Appl. Phys.* **101**, 093105 (2007).
12. Gu, Q. L. Plasmonic metallic nanostructures for efficient absorption enhancement in ultrathin CdTe-based photovoltaic cells. *J. Phys. D: Appl. Phys.* **43**, 465101 (2010).
13. Kang, M. G., Xu, T., Park, H. J., Luo, X. G. & Guo, L. J. Efficiency enhancement of organic solar cells using transparent plasmonic Ag nanowire electrodes. *Adv. Mater.* **22**, 4378–4383 (2010).
14. Brown, M. D. *et al.* Plasmonic dye-sensitized solar cells using core-shell metal-insulator nanoparticles. *Nano Lett.* **11**, 438–445 (2011).
15. Ko, D. H. *et al.* Photonic crystal geometry for organic solar cells. *Nano Lett.* **9**, 2742–2746 (2009).
16. Nishimura, S. *et al.* Standing wave enhancement of red absorbance and photocurrent in dye-sensitized titanium dioxide photoelectrodes coupled to photonic crystals. *J. Am. Chem. Soc.* **125**, 6306–6310 (2003).
17. Lozano, G., Colodrero, S., Caulier, O., Calvo, M. E. & Míguez, H. N. Theoretical analysis of the performance of one-dimensional photonic crystal-based dye-sensitized solar cells. *J. Phys. Chem. C* **114**, 3681–3687 (2010).
18. Calvo, M. E. *et al.* Porous one dimensional photonic crystals: novel multifunctional materials for environmental and energy applications. *Energy Environ. Sci.* **4**, 4800–4812 (2011).
19. Suezaki, T., Yano, H., Hatayama, T., Ozin, G. A. & Fuyuki, T. Photoconductivity in inverse silicon opals enhanced by slow photon effect: Yet another step towards optically amplified silicon photonic crystal solar cells. *Appl. Phys. Lett.* **98**, 072106 (2011).
20. Catchpole, K. R. *et al.* Plasmonics and nanophotonics for photovoltaics. *MRS Bull.* **36**, 461–467 (2011).
21. Kim, J., Koh, J. K., Kim, B., Kim, J. H. & Kim, E. Nanopatterning of mesoporous inorganic oxide films for efficient light harvesting of dye-sensitized solar cells. *Angew. Chem. Int. Ed.* **124**, 6970–6975 (2012).
22. Guldin, S. *et al.* Dye-sensitized solar cell based on a three-dimensional photonic crystal. *Nano Lett.* **10**, 2303–2309 (2010).
23. Colodrero, S. *et al.* Efficient transparent thin dye solar cells based on highly porous 1D photonic crystals. *Adv. Funct. Mater.* **22**, 1303–1310 (2012).
24. Guo, M. *et al.* Design and coupling of multifunctional TiO_2 nanotube photonic crystal to nanocrystalline titania layer as semi-transparent photoanode for dye-sensitized solar cell. *Energy Environ. Sci.* **5**, 9881–9888 (2012).
25. Yip, C. T. *et al.* Direct and seamless coupling of TiO_2 nanotube photonic crystal to dye-sensitized solar cell: a single-step approach. *Adv. Mater.* **23**, 5624–5628 (2011).
26. Feng, J., Qian, X., Huang, C.-W. & Li, J. Strain-engineered artificial atom as a broad-spectrum solar energy funnel. *Nat. Photon.* **6**, 866–872 (2012).
27. Macia, E. Exploiting aperiodic designs in nanophotonic devices. *Rep. Prog. Phys.* **75**, 036502 (2012).
28. Arie, A. & Voloch, N. Periodic, quasi-periodic, and random quadratic nonlinear photonic crystals. *Laser Photonics Rev.* **4**, 355–373 (2010).
29. Macia, E. & DominguezAdame, F. Can fractal-like spectra be experimentally observed in aperiodic superlattices? *Semicond. Sci. Tech.* **11**, 1041–1045 (1996).
30. Endo, A. & Iye, Y. Fourier analyses of commensurability oscillations in Fibonacci lateral superlattices. *Phys. Rev. B* **78**, 085311 (2008).
31. Hsueh, W. J., Chen, C. H. & Lai, J. A. Splitting rules of electronic miniband in Fibonacci superlattices: a gap map approach. *Eur. Phys. J. B* **73**, 503–508 (2010).
32. Grätzel, M. Recent Advances in Sensitized Mesoscopic Solar Cells. *Acc. Chem. Res.* **42**, 1788–1798 (2009).
33. Zhu, K., Neale, N. R., Miedaner, A. & Frank, A. J. Enhanced charge-collection efficiencies and light scattering in dye-sensitized solar cells using oriented TiO_2 nanotubes arrays. *Nano Lett.* **7**, 69–74 (2006).

Acknowledgments

This work is fully supported by grants received from the Research Grants Council of the Hong Kong Special Administrative Region (Project Nos.: PolyU5163/12E, PolyU5159/13E and PolyU152057/14E) and grant from the Hong Kong Polytechnic University (Project No.: RT5W). K.Y.X. is grateful for the financial support from the National Natural Science Foundation of China (No.51302219), the Specialized Research Fund for the Doctoral Program of Higher Education of China (No.20136102120024 and 20136102140001) and the Fundamental Research Funds for the Central Universities (No. 3102014JCQ01019). W.Y. thanks the support from the National High Technology Research and Development Program of China (863 Program) (No.2013AA031903). The authors thank Prof. Wing Yim Tam and Ms. Jenny Hung for assistance in reflectance measurement. The authors would also like to thank Mr. Zehui Yong for helpful discussions on the modeling.

Author contributions

H.H. conceived the idea. H.H. and K.X. designed the experiments. M.G. and K.X. fabricated the samples and carried out the experiments. M.G. did the simulation. K.X., M.G. and H.H. wrote the paper. H.H., G.M., K.X., Y.W., and L.Z. analyzed the experiment data and discussed the results.

Additional information

Supplementary information accompanies this paper at http://www.nature.com/scientificreports

Competing financial interests: The authors declare no competing financial interests.

How to cite this article: Guo, M., Xie, K., Wang, Y., Zhou, L. & Huang, H. Aperiodic TiO_2 Nanotube Photonic Crystal: Full-Visible-Spectrum Solar Light Harvesting in Photovoltaic Devices. *Sci. Rep.* **4**, 6442; DOI:10.1038/srep06442 (2014).